ACS Energy LETTERS

http://pubs.acs.org/journal/aelccp

Predicted Operando Polymerization at Lithium Anode via Boron Insertion

Yue Liu, Peiping Yu, Qintao Sun, Yu Wu, Miao Xie, Hao Yang, Tao Cheng,* and William A. Goddard, III

Cite This: *ACS Energy Lett.* 2021, 6, 2320−2327

Read Online

ACCESS | Metrics & More | Article Recommendations | Supporting Information

ABSTRACT: Concentrated dual-salt/ester systems have been demonstrated as an effective method in regulating the solid electrolyte interphase (SEI) formation that facilitates the long-term cycling stability of lithium metal batteries (LMBs). However, the atomic mechanism of the dual-salt enabling the stable SEI formation remains unclear. In this work, a hybrid scheme, combining ab initio and reactive force field methods (HAIR), is employed to investigate the initial reaction of SEI formation by monitoring 1 ns molecular dynamics (MD) simulation. The simulation results reveal that lithium bis(trifluoromethanesulfonyl)imide (LiTFSI) is subject to a sacrificial decomposition to protect lithium difluoro(oxalato)borate (LiDFOB) from being over-reduced by Li metal. The boron (B) released from LiDFOB can initiate a polymerization reaction by cutting the C−O bond. Such unexpected reaction turns dimethoxyethane (DME), a previously considered stable solvent, into a radical that can facilitate the propagation of polymerization. These insights from simulation provide atomic understanding about the complex reaction in SEI.

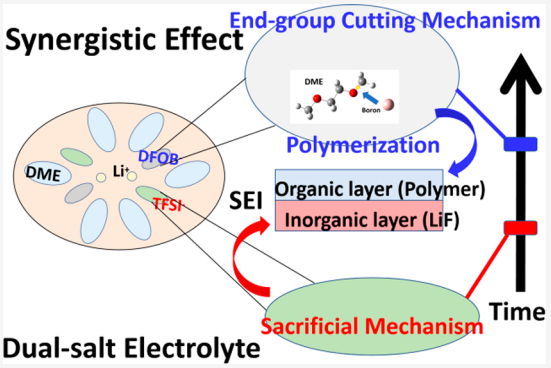

As the demand for renewable energy continues to proliferate, conventional lithium-ion batteries (LIBs), consisting of a graphite anode and a Li^+ intercalation/deintercalation cathode, have reached their theoretical specific capacity of 372 mAh g^{-1}, which is far from satisfying the continuous requirements in the field of high-energy storage.[1−4] A state-of-art alternative method to obtain ultrahigh energy density replaces the graphite anode with ideal lithium metal material, which possesses a specific capacity of 3860 mAh g^{-1} and a low electrochemical potential of −3.040 V, namely, lithium metal batteries (LMBs).[5−7] Although it is theoretically feasible to replace the graphite anode with Li metal anode, obstacles prevent LMBs from large-scale commercialization nowadays. For instance, the high reactivity property of Li metal leads to heterogeneous dendrite growth through the reductive reaction of electrolyte, and dendrite could even pierce the membrane, which causes serious safety concerns.[8,9] Besides, the irreversible deposition of Li metal results in dead lithium layer formation, which dramatically reduces Coulombic efficiencies (CEs) and worsens cycling performance.[10,11] Therefore, these uncontrollable challenges greatly limit the development and application of LMBs.

Solid-electrolyte interphase (SEI), serving as a passivation layer on Li metal anode, has been recognized to dictate the reactivity of Li metal anode to affect the CEs and performance of LMBs further.[12,13] To optimize the performance of LMBs by adjusting the SEI formation process, one of the most effective methods is to manipulate the nature of the electrolyte, such as high concentration (HC) electrolyte with additives.[14−17] Suo[18] proposed an HC (up to 7 mol·kg^{-1}) electrolyte system where, for dissolved lithium bis(trifluoromethanesulfonyl)imide (LiTFSI) salt in the mixed solvents of dimethoxyethane (DME) and dioxalane (DOL) in Li/S batteries, the stability of the Li metal anode is significantly enhanced in comparison with the conventional electrolyte of 1 mol·L^{-1}. Yamada[19] calculated the lowest unoccupied molecular orbital (LUMO) of TFSI ion with density functional theory (DFT). They found the LUMO of TFSI is lower than that of solvent in HC electrolyte, indicating that the TFSI ion is formed before reduction with SEI layer. The oxidation stability of solvent is also enhanced due to Li-solvent pairs formation in the HC system. These theoretical results clarified why the concentration of Li-salt could improve the stability of Li metal anode.

Received: May 2, 2021
Accepted: May 27, 2021
Published: June 1, 2021

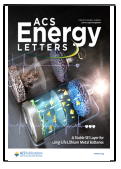

https://doi.org/10.1021/acsenergylett.1c00907
ACS Energy Lett. 2021, 6, 2320−2327

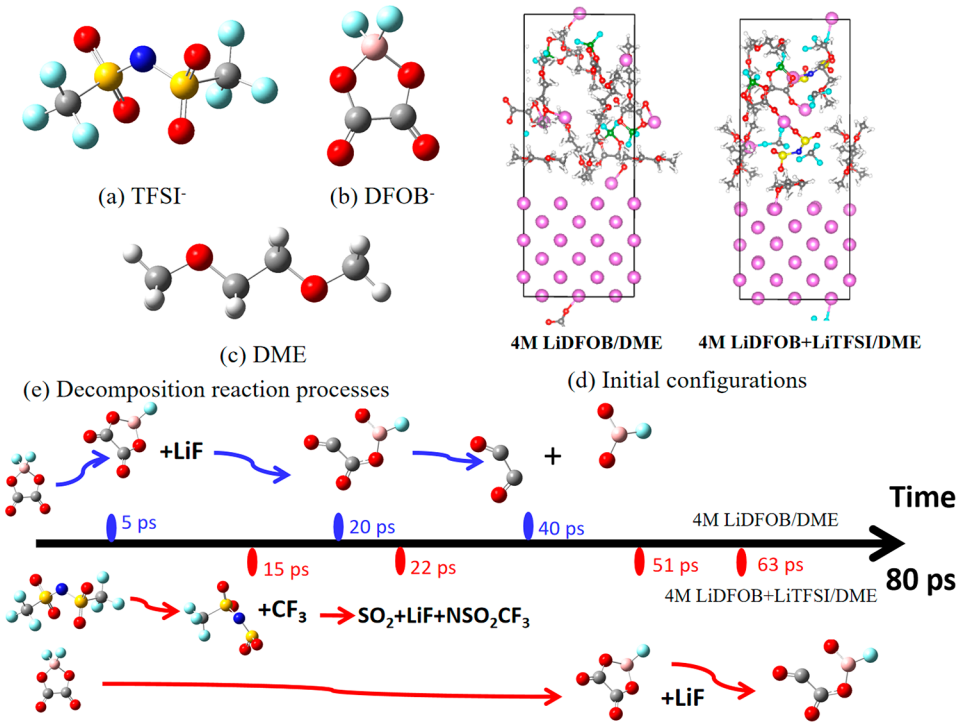

Figure 1. Geometries for (a) TFSI ion, (b) DFOB ion, and (c) DME; (d) initial configurations for 4 M LiDFOB/DME and LiDFOB +LiTFSI/DME systems; (e) decomposition reaction processes for TFSI and DFOB ions obtained from AIMD simulation for 4 M LiDFOB/ DME and 4 M LiDFOB+LiTFSI/DME systems. Color code: lithium, purple; oxygen, red; carbon, gray; fluorine, cyan; sulfur, yellow; nitrogen, blue; boron, pink; hydrogen, white.

Besides, Qian[20] investigated the growth process of lithium dendrite in different electrolytes. They concluded that the high concentration of lithium bis(fluorosulfonyl)imide (LiFSI)/ DME electrolyte could effectively inhibit uncontrolled dendrite growth and significantly improve the CEs of batteries. To elucidate the effects with different concentrations of Li salts, Camacho-Forero[21] performed ab initio molecular dynamics (AIMD) simulations to explore the LiTFSI and LiFSI decomposition processes at 1 and 4 M concentrations within 20 ps; specific structural-, dynamical-, and reactivity-associated issues at 4 M concentration point to the initial SEI formation process.

Although HC (7 M LiTFSI) systems pose peculiar physicochemical properties and outstanding electrochemical performance in stabilizing the Li-metal anode, the high electrolyte concentration still brings a series of problems such as high viscosity and high cost. More recently, a concentrated dual salt/ether electrolyte, which induces the SEI formation, was designed by Jiao et al.[22] The 2 mol·L^{-1} lithium difluoro(oxalato)borate LiDFOB with 2 mol·L^{-1} LiTFSI/DME system exhibits outstanding performance with a capacity retention of >90% over 300 cycles and ∼80% over 500 cycles. A scanning electron microscope (SEM) is used to characterize cycled Li metal anode. A high-quality SEI layer is formed in the dual-salt system compared with the other two electrolytes (4 M LiDFOB/DME and 3 M LiTSFI/DME). X-ray photoelectron spectroscopy (XPS) and Fourier transform infrared (FTIR) spectra are also performed, which implied that dual-salt decomposition might contribute to forming a thin and dense SEI layer. Consequently, although some experimental methods could characterize the components of SEI formation, the reductive degradation mechanism and the role of dual-salt played in the SEI formation process are still unclear, which provide prospective insights for further SEI layer design.

Molecular dynamics (MD) simulation technologies based on quantum mechanics (QM) or molecular mechanics (MM) methods have been considered promising tools to explore complex reaction processes by monitoring MD trajectories at the atomic level.[23,24] DFT-based AIMD simulations are suitable for describing the initial reactions within 10's of picoseconds (ps). In contrast, long-time SEI formation simulations are hard to be achieved due to their expensive computational cost.[25] Reactive force field, comprising different energy parts based on defining bond-order, has been regarded as an efficient MM method to describe the bond formation and cleavage processes with a relatively low cost, which is beneficial for extending the time-scale of ReaxFF MD simulation to nanoseconds (ns) or microseconds (μs).[26−29] Despite the eReaxFF framework developed to overcome the lack of considering the explicit electron in the conventional ReaxFF method, eReaxFF has not yet been adequate for the above systems.[30,31] Li-ion transfer energetics through the electrode/ SEI/electrolyte interface are investigated using the density functional based tight-binding (DFTB) method, offering an efficient approach using a second-order expansion of the Kohn−Sham total energy in DFT concerning charge density fluctuations.[32]

Hybrid ab initio and reactive force field methods (HAIR) are used in this work, which seems to be a promising candidate to keep a good balance of computational efficiency and accuracy. The hybrid method employs AIMD simulations coupled with ReaxFF MD. AIMD simulations exhibit accurate descriptions for the localized electrochemical reactions, and the ReaxFF MD simulations accelerate chemical reactions and the mass transfer in the meantime.[33,34] In this work, we build the

https://doi.org/10.1021/acsenergylett.1c00907
ACS Energy Lett. 2021, 6, 2320−2327

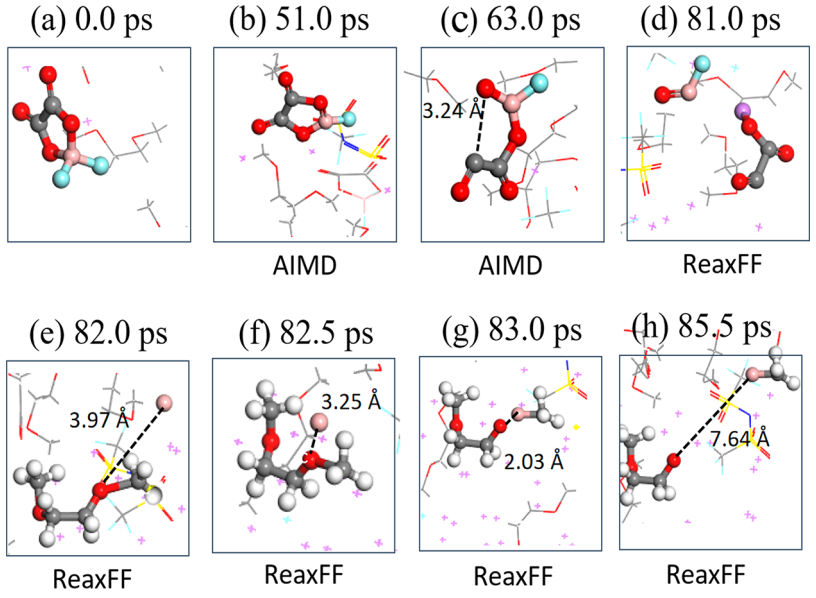

Figure 2. Sequence of DFOB and DME decomposition obtained from AIMD (80 ps) and HAIR simulations for dual-salt system between 80 and 85.5 ps: (a) 0.0 ps; (b) 51.0 ps; (c) 63.0 ps; (d) 81.0 ps; (e) 82.0 ps; (f) 82.5 ps; (g) 83.0 ps; (h) 85.5 ps. Color codes are as indicated in Figure 1.

single- and dual-salt systems in experiments: LiTFSI/DME, LiDFOB/DME, and LiTFSI+LiDFOB/DME system. To obtain the reliable initial reductive reaction processes, AIMD simulations are performed for 80 ps. Subsequently, HAIR simulations are conducted with 10−20 times acceleration for long-time simulations (∼1 ns).

The Li-metal anode is represented by a six-layer (3 × 3) supercell slab with Li (100) surface to model the Li metal anode and electrolyte system.[35] The concentrated dual/ester electrolyte is constructed with two molecules of LiDFOB and two molecules of LiTFSI dissolved in six molecules of DME, which shows the approach to achieve 4 M LiDFOB+LiTFSI/DME electrolyte system as designed experimentally. Moreover, the theoretical models for single-salt systems are also constructed as a dual-salt system, 4 M LiDFOB/DME and 3 M LiTFSI/DME, respectively.

The initial reaction mechanisms are performed with AIMD for 80 ps using the Vienna ab Initio Simulation Package (VASP 5.4.4).[36] Perdew−Burke−Ernzerhof (PBE) functional is used to describe the electron exchange, and correction energies within the generalized gradient approximation (GGA) and London dispersion integrations are described using Grimme D3 correction.[37,38] To sample Brillouin zone integration,[39] a 1 × 1 × 1 Monkhorst−Pack k-point mesh and a 400 eV energy cutoff are used for plane-wave basis expansion. Besides, the projector augmented wave (PAW) method[40] is conducted in this work. To guarantee reliable AIMD results, 0.2 eV width of Gaussian smearing and 10^{-4} eV width are used as electronic structure convergence. To conduct the X-ray photoelectron spectroscopy (XPS) analysis, the binding energies are calculated by initial state approximation using VASP at the PBE-D3 level.

During HAIR simulations, AIMD simulations coupled with ReaxFF MD are employed alternately, which last 0.5 and 5 ps for AIMD and ReaxFF, respectively, with factors of 10 and 20. All MD simulations are performed with the *NVT* ensemble at 300 K, and the ReaxFF procedure is performed using Large-Scale Atomic/Molecular Massively Parallel Simulator (LAMMPS 2018) software.[41] To get exemplary energy conservation and efficient converge for collisions, we used 1 fs time step in AIMD while 0.25 fs time step was used for ReaxFF.

Figure 1 shows the snapshots from AIMD simulations for 4 M LiDFOB/DME and 4 M LiDFOB+LiTFSI/DME systems. In 4 M LiDFOB/DME, DFOB ion decomposition is initiated via B−F cleavage by Li^0 at around 5 ps and then ring-opened through C−O bond breaking. To clarify the differences in dual-salt electrolytes, we found that TFSI is more easily reduced than DFOB via C−S bond breaking, preventing the DFOB from being ring-opened, exhibited in Figure 1e. The TFSI ion undergoes C−S and N−S bond cleavages from 15 to 22 ps, the same as in our previous work.[33] The DFOB ion starts to reduce by Li^0 at 51 ps via B−F bond breaking, which is much slower than in the LiDFOB/DME system, indicating that the TFSI in the dual-salt system is before reducing with the consumption of free Li^0. A similar sacrificial reaction mechanism could be summarized as proposed by Sodeyama,[42] which elucidates the reasons behind the switch from solvent-derived to salt-derived SEI formation process in high concentration electrolyte systems.

As the initial reaction mechanism obtained from AIMD simulation results, synergistic effects are worth to be explored to clarify the role of LiTFSI and LiDFOB salts played in the concentrated dual-salts system. Consequently, further reactions need to be investigated with the HAIR simulation method proposed to extend the time-scale from picosecond to nanosecond. The final MD simulations of single and dual-salt systems are shown in Figure S1. During the initial 100 ps, the reductive decomposition mechanisms of LiDFOB and solvent DME are clarified, while the decomposition of LiTFSI shows no differences with previous work.[21,33] As is shown in Figure 2a−d, the DFOB ion is reduced by Li^0 to form LiF via B−F bond breaking. Subsequently, the C−O bond is elongated at 3.24 Å, indicating the ring-opened process is observed by C−O bond cleavage in AIMD simulations. After that, a further

https://doi.org/10.1021/acsenergylett.1c00907
ACS Energy Lett. 2021, 6, 2320−2327

decomposition process happens with release of a free boron atom, which plays an essential role in further reducing DME.

Figure 2e−h exhibits the detailed MD trajectories of DME decomposition, and we found a new boron insertion process. Boron atom inserts into the C−O bond and then releases with the B−CH_3 fragment, initiating DME reduction. To further realize the boron insertion process, the QM method calculates the Gibbs free energies at the B3LYP/6-311+g(d,p) level using Jaguar 8.8. As the Gibbs free energies are shown in Figure S2, the reaction between DME and Li_x−B is significantly favorable via C−H and C−O bond insertions, suggesting that the boron insertion processes are thermodynamically possible. The relative reaction energies implied that the insertion reaction tends to insert a C−O bond rather than a C−H bond to form $CH_3OCH_2CH_2O$ as predicted by MD simulations.

On the basis of the QM and MD results, a new mechanism is proposed in this work, denoted as the "end-group cutting mechanism" (Figure 3). Owing to the saturated bonds and the stable end methyl group in DME, it is known that the DME molecule shows chemical stability and inertness. The solvent DME, initiated by boron atom via C−O insertion process to "cut off" end methyl group, is reduced in the dual-salt electrolyte system, considered the initial critical reaction (end-group cutting mechanism) to activate the DME reduction process. A similar boron-attacking reaction process has also been proposed in Jiao's work.[22] They suggested that the boron atom release from LiDFOB has a tendency to coordinate with electron-rich species, initiating polymerization reactions, and Fourier transform infrared (FTIR) spectra verify these hypotheses.

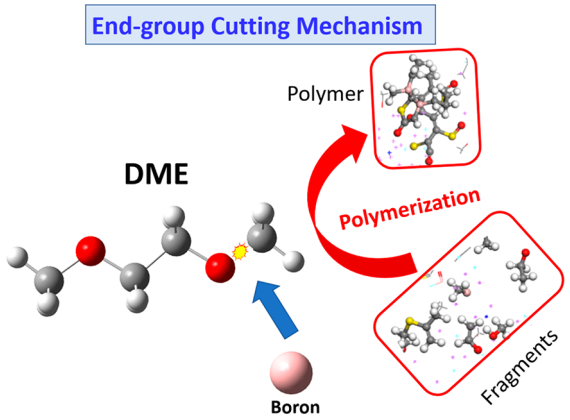

Figure 3. Schematic diagram of end-group cutting mechanism.

Furthermore, single- and dual-salt electrolytes are investigated using the HAIR method after 1 ns long MD simulations (which contain a 10 times factor for 550 ps and 20 times factor for 450 ps HAIR simulations, respectively). It is worth mentioning that only one DME molecule is reduced in the single-salt electrolyte (4 M LiDFOB/DME and 3 M LiTFSI/DME), and no end-group cutting mechanism is observed (Figure S3). In contrast, almost all DME solvents are reduced by boron atoms at the dual-salt system. Figure 4 shows the sequence of polymerization reactions in a dual-salt electrolyte system, the $CH_3OCH_2CH_2O$ and salt decomposed into various species, and the cross-linking polymerization reactions happen after 1 ns gradually. As for the 3 M LiTFSI/DME systems, it is evident that no decomposition of DME is seen due to the lack of a boron atom, as expected, while in 4 M LiDFOB/DME, boron atoms, released from the decomposition of LiDFOB, are coordinated by Li^0 quickly without the protection of LiTFSI, which prevents the reductive reaction of DME initiated by boron. The dual salt shows unique processes in the reduction of electrolytes. LiTFSI decomposes with the consumption of free Li^0 sacrificially, and then further release of boron atoms in LiDFOB contributes to reducing the solvents DME. On the basis of the theoretical observation and

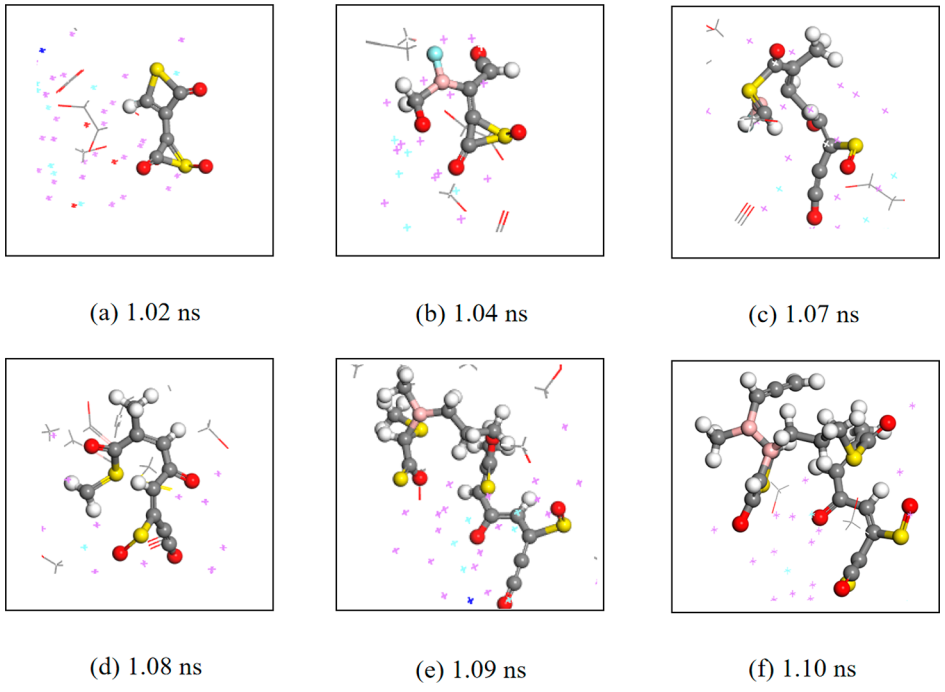

Figure 4. Sequence of polymerization reactions obtained from HAIR simulations for dual-salt system after 1 ns: (a) 1.02 ns; (b) 1.04 ns; (c) 1.07 ns; (d) 1.08 ns;(e) 1.09 ns; (f) 1.10 ns. Color codes are as indicated in Figure 1.

https://doi.org/10.1021/acsenergylett.1c00907
ACS Energy Lett. 2021, 6, 2320−2327

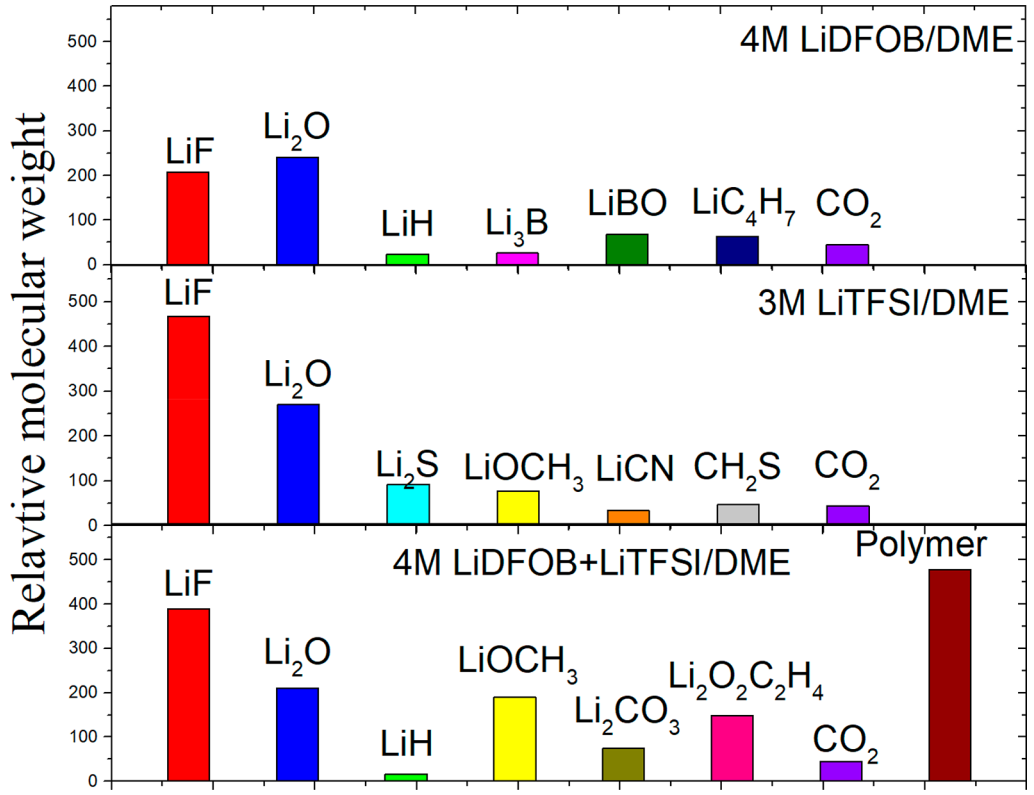

Figure 5. Relative mass ratio of main products after 1 ns HAIR MD simulation for 4 M LiDFOB/DME, 3 M LiTFSI/DME, and 4 M LiDFOB +LiTFSI/DME systems.

reduction mechanism, synergistic effects of concentrated dual-salt/ether electrolyte are clarified to reveal the reason behind the chemical phenomena. In the dual-salt system, LiTFSI is before reducing the consumption of free Li^0 to protect LiDFOB. The sacrificial mechanism is predicted because LiTFSI supplies much more atoms than LiDFOB to coordinate with Li, such as F and O atoms. Subsequently, the decomposition of LiDFOB would release boron atom, which is devoted to initiating DME decomposition by cutting off the end methyl group. Their theoretical results indicate none of them could achieve the synergistic effects.

To investigate the composition of SEI layers obtained from HAIR simulations, Figure 5 and Figure S4 exhibit the relative molecular weight and numbers of main products for 4 M LiDFOB/DME, 3 M LiTFSI/DME, and 4 M LiDFOB +LiTFSI/DME systems. In the LiDFOB/DME system, the main products include LiF, Li_2O, and Li_3B, LiBO, which are derived from the decomposition of LiDFOB. As for the LiTFSI/DME electrolyte, the LiF molecule shows an overwhelming number compared with any other products due to F atoms released from LiTFSI. Additionally, the dual-salt system poses a large number of LiF compounds, and some organic products are also seen due to the reductive reaction of DME. For example, $LiOCH_3$ and $Li_2O_2C_2H_4$ are observed, formed via the "end-group cutting mechanism" to generate OCH_3 and $C_2H_4O_2$. The free boron atom can initiate the reduction of DME and induce cross-linking or polymerization reactions as observed by Jiao[22] with the Fourier transform infrared (FTIR) spectra method. Similar reactions and products are also observed from our MD simulations, as shown in Figure 4f, suggesting the long-chain polymer has a cross-linking structure through B−C bonds. In the SEI layer formed in the dual-salt electrolyte, LiF and polymer are the main inorganic and organic layers, respectively, as the relative molecular weights predicted. Some of the geometries obtained from the MD simulation are exhibited in Figure S5.

Figure S6 shows the radial distribution function (RDF) and integrated number of bonds for single- and dual-salt systems. The RDF results for Li−F and Li−O imply that the main products are LiF and Li_2O, and the numbers of Li−F and Li−O bonds in the dual-salt system are between the single-salt systems. Concerning Li−B and B−C bonds, we compare the 4 M LiDFOB/DME and 4 M LiDFOB+LiTFSI/DME systems and boron atoms are before coordinating with Li in 4 M LiDFOB/DME as the RDF. The integrated number of Li−B bonds is predicted in Figure S6c. Simultaneously, a sharp peak is observed in the dual-salt system in Figure S6d, indicating the formation of the B−C bond in cross-linking polymerization reactions.

The HAIR scheme can increase the computational efficiency significantly, 10−100 times, which allows extending the ab initio investigation of initial reactions of SEI formation.[33,34] However, the new time scale, ∼1 ns, is still not sufficient to fully capture the complete reaction pathway to products, which will require further development in multiscale simulation techniques specified for battery simulations.

To simulate the XPS spectra of single- and dual-salt electrolytes, structures from MD simulations are used to calculate the binding energies. The statistical distributions are fitted with the Gaussian function in Figure 6.[43] According to the binding energies of Li−F, C−F, and B−F, the binding energy shift of C−F to Li−F is 3.8 eV in the 3 M LiTFSI/DME electrolyte. The corresponding value is 3.9 eV predicted in Jiao's experimental work.[22] As for the B−F to Li−F in

https://doi.org/10.1021/acsenergylett.1c00907
ACS Energy Lett. 2021, 6, 2320−2327

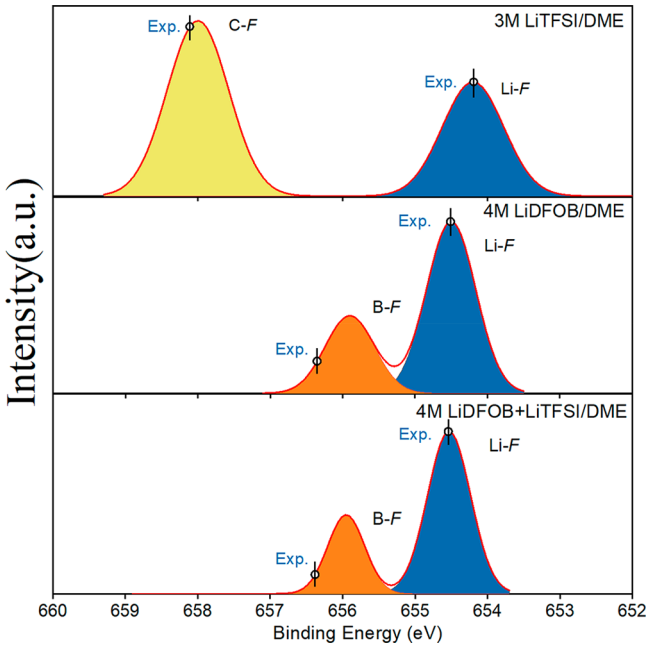

Figure 6. XPS spectra of F 1s in 4 M LiDFOB/DME, 3 M LiTFSI/DME, and 4 M LiDFOB+LiTFSI/DME systems. Experimental binding energy shift of C−F and B−F to Li−F are marked with dots, from ref 22.

LiDFOB/DME and LiDFOB+LiTFSI/DME systems, the binding energy shift is 1.5 eV compared to the experimental result of 1.9 eV.[22] Besides, the dual-salt exhibits a narrower peak in Li−F, which suggests a homogeneous inorganic layer may be formed.

In summary, synergistic effects of the dual-salt system are clarified using the hybrid ab initio and reactive force field reactive dynamics (HAIR) method, showing good agreements with experimental results. Detailed reductive reaction mechanisms of electrolytes are explored by monitoring MD trajectories. The dual-salt system poses synergistic effects of two salts, which play different but complementary roles in the SEI formation process. LiTFSI decomposes via a "sacrificial mechanism" to protect LiDFOB, preventing boron atoms from coordination by free Li^0. The boron atom is derived from the decomposition of LiDFOB, initiating the "end-group cutting mechanism" to reduce DME solvents. These reaction mechanisms are verified by QM calculations and analyzed by product distributions and RDF results. It is possible to validate the proposed reaction mechanism by combining cryoelectron microscopy with accurate detection of boron (say with NMR). Although not practical now, such characterization is promising for the near future.

Furthermore, the reductive reaction between a boron atom and DME, leading to a cross-linking polymerization process, and the long-chain polymer product are observed as mentioned in experiments.[22] The binding energy shifts of B−F to Li−F and C−F to Li−F are predicted to be 1.5 and 3.8 eV with XPS spectra, compared with 1.9 and 3.9 eV experimentally.[22] XPS results indicate that a homogeneous inorganic (LiF) layer is formed in a dual-salt system. These theoretical results provide evidence for the synergistic effects of advanced dual-salt electrolytes, which offer new insights in developing long-term cycling stability batteries.

Further development in understanding the atomic structure of SEI relies on both experiment and theory, especially the close collaboration from both ends.

■ ASSOCIATED CONTENT

Supporting Information

The Supporting Information is available free of charge at https://pubs.acs.org/doi/10.1021/acsenergylett.1c00907.

Snapshots from HAIR MD simulation after 1 ns for single- and dual-salt systems (Figures S1 and S3); reaction and relative Gibbs free energies between DME and Li_x-B (Figure S2); numbers of main products after 1 ns with the different system (Figure S4); geometries of products obtained from MD simulations directly (Figure S5); radial distribution function and integrated number of bonds for Li−F, Li−O, Li−B, B−C after 1 ns HAIR simulations (Figure S6); XRD patterns from MD simulations (Figure S7); details for the HAIR method and force field development (Figures S8−S10 and Tables S1 and S2) (PDF)

■ AUTHOR INFORMATION

Corresponding Author

Tao Cheng − *Institute of Functional Nano and Soft Materials (FUNSOM), Soochow University, Suzhou 215123, China;* orcid.org/0000-0003-4830-177X; Email: tcheng@suda.edu.cn

Authors

Yue Liu − *Institute of Functional Nano and Soft Materials (FUNSOM), Soochow University, Suzhou 215123, China*

Peiping Yu − *Institute of Functional Nano and Soft Materials (FUNSOM), Soochow University, Suzhou 215123, China*

Qintao Sun − *Institute of Functional Nano and Soft Materials (FUNSOM), Soochow University, Suzhou 215123, China*

Yu Wu − *Institute of Functional Nano and Soft Materials (FUNSOM), Soochow University, Suzhou 215123, China*

Miao Xie − *Institute of Functional Nano and Soft Materials (FUNSOM), Soochow University, Suzhou 215123, China;* orcid.org/0000-0002-9797-1449

Hao Yang − *Institute of Functional Nano and Soft Materials (FUNSOM), Soochow University, Suzhou 215123, China;* orcid.org/0000-0002-8241-6231

William A. Goddard, III − *Materials and Process Simulation Center, Department of Chemistry, California Institute of Technology, Pasadena, California 91125, United States;* orcid.org/0000-0003-0097-5716

Complete contact information is available at: https://pubs.acs.org/10.1021/acsenergylett.1c00907

Notes

The authors declare no competing financial interest.

■ ACKNOWLEDGMENTS

T.C. and M.X. thank the National Natural Science Foundation of China (Grants 21903058 and 22003044), the Natural Science Foundation of Jiangsu Higher Education Institutions (Grant SBK20190810), the Jiangsu Province High-Level Talents (Grant JNHB-106), and the Priority Academic Program Development of Jiangsu Higher Education Institutions (PAPD) for financial support. H.Y. thanks China Postdoctoral Science Foundation (Grant 2019M660128) for

financial support. This work was partly supported by the Collaborative Innovation Center of Suzhou Nano Science & Technology. W.A.G. gratefully acknowledges support from NSF (Grant CBET-1805022). We thank Dr. Shuhong Jiao and Ruiguo Cao for fruitful discussions about the experiments.

REFERENCES

(1) Goodenough, J. B.; Park, K. S. The Li-Ion Rechargeable Battery: A Perspective. *J. Am. Chem. Soc.* **2013**, *135*, 1167−1176.
(2) Cheng, X. B.; Zhang, R.; Zhao, C. Z.; Zhang, Q. Toward Safe Lithium Metal Anode in Rechargeable Batteries: A Review. *Chem. Rev.* **2017**, *117*, 10403−10473.
(3) Tarascon, J. M.; Armand, M. Issues and Challenges Facing Rechargeable Lithium Batteries. *Nature* **2001**, *414*, 359−367.
(4) Dunn, B.; Kamath, H.; Tarascon, J.-M. Electrical Energy Storage for the Grid: A Battery of Choices. *Science* **2011**, *334*, 928−935.
(5) Zheng, J. M.; Engelhard, M. H.; Mei, D. H.; Jiao, S. H.; Polzin, B. J.; Zhang, J. G.; Xu, W. Electrolyte Additive Enabled Fast Charging and Stable Cycling Lithium Metal Batteries. *Nat. Energy* **2017**, *2*, 17012.
(6) Xu, W.; Wang, J. L.; Ding, F.; Chen, X. L.; Nasybulin, E.; Zhang, Y. H.; Zhang, J. G. Lithium Metal Anodes for Rechargeable Batteries. *Energy Environ. Sci.* **2014**, *7*, 513.
(7) Lin, D. C.; Liu, Y. Y.; Cui, Y. Reviving the Lithium Metal Anode for High-Energy Batteries. *Nat. Nanotechnol.* **2017**, *12*, 194−206.
(8) Shi, F. F.; Pei, A.; Boyle, D. T.; Xie, J.; Yu, X. Y.; Zhang, X. K.; Cui, Y. Lithium Metal Stripping Beneath the Solid Electrolyte Interphase. *Proc. Natl. Acad. Sci. U. S. A.* **2018**, *115*, 8529−8534.
(9) Huang, C.; Xiao, J.; Shao, Y. Y.; Zheng, J. M.; Bennett, W. D.; Lu, D. P.; Saraf, L. V.; Engelhard, M.; Ji, L. W.; Zhang, J. G.; et al. Manipulating Surface Reactions in Lithium-Sulphur Batteries Using Hybrid Anode Structures. *Nat. Commun.* **2014**, *5*, 3015.
(10) Ding, F.; Xu, W.; Chen, X. L.; Zhang, J.; Engelhard, M. H.; Zhang, Y. H.; Johnson, B. R.; Crum, J. V.; Blake, T. A.; Liu, X. J.; et al. Effects of Carbonate Solvents and Lithium Salts on Morphology and Coulombic Efficiency of Lithium Electrode. *J. Electrochem. Soc.* **2013**, *160*, A1894−A1901.
(11) Scheers, J.; Fantini, S.; Johansson, P. A Review of Electrolytes for Lithium−Sulphur Batteries. *J. Power Sources* **2014**, *255*, 204−218.
(12) Li, S.; Jiang, M. W.; Xie, Y.; Xu, H.; Jia, J. Y.; Li, J. Developing High-Performance Lithium Metal Anode in Liquid Electrolytes: Challenges and Progress. *Adv. Mater.* **2018**, *30*, 1706375.
(13) Xu, K. Electrolytes and Interphases in Li-ion Batteries and Beyond. *Chem. Rev.* **2014**, *114*, 11503−11618.
(14) Jie, Y. L.; Ren, X. D.; Cao, R.; Cai, W. B.; Jiao, S. H. Advanced Liquid Electrolytes for Rechargeable Li Metal Batteries. *Adv. Funct. Mater.* **2020**, *30*, 1910777.
(15) Ueno, K.; Yoshida, K.; Tsuchiya, M.; Tachikawa, N.; Dokko, K.; Watanabe, M. Glyme-Lithium Salt Equimolar Molten Mixtures: Concentrated Solutions or Solvate Ionic Liquids? *J. Phys. Chem. B* **2012**, *116*, 11323−11331.
(16) Zhang, X. Q.; Chen, X.; Cheng, X. B.; Li, B. Q.; Shen, X.; Yan, C.; Huang, J. Q.; Zhang, Q. Highly Stable Lithium Metal Batteries Enabled by Regulating the Li^+ Solvation in Nonaqueous Electrolyte. *Angew. Chem., Int. Ed.* **2018**, *57*, 5301.
(17) Yamada, Y.; Yaegashi, M.; Abe, T.; Yamada, A. A Super-Concentrated Ether Electrolyte for Fast-Charging Li-Ion Batteries. *Chem. Commun.* **2013**, *49*, 11194−11196.
(18) Suo, L. M.; Hu, Y.-S.; Li, H.; Armand, M.; Chen, L. Q. A New Class of Solvent-in-Salt Electrolyte for High-Energy Rechargeable Metallic Lithium Batteries. *Nat. Commun.* **2013**, *4*, 1481.
(19) Yamada, Y.; Furukawa, K.; Sodeyama, K.; Kikuchi, K.; Yaegashi, M.; Tateyama, Y.; Yamada, A. Unusual Stability of Acetonitrile-Based Superconcentrated Electrolytes for Fast-Charging Lithium-Ion Batteries. *J. Am. Chem. Soc.* **2014**, *136*, 5039−5046.
(20) Qian, J. F.; Henderson, W. A.; Xu, W.; Bhattacharya, P.; Engelhard, M.; Borodin, O.; Zhang, J. G. High Rate and Stable Cycling of Lithium Metal Anode. *Nat. Commun.* **2015**, *6*, 6362.
(21) Camacho-Forero, L. E.; Smith, T. W.; Balbuena, P. B. Effects of High and Low Salt Concentration in Electrolytes at Lithium−Metal Anode Surfaces. *J. Phys. Chem. C* **2017**, *121*, 182−194.
(22) Jiao, S. H.; Ren, X. D.; Cao, R. G.; Engelhard, M. H.; Liu, Y.; Hu, D. H.; Mei, D. H.; Zheng, J. M.; Zhao, W.; Li, Q. Y.; Liu, N.; Adams, B. D.; Ma, C.; Liu, J.; Zhang, J. G.; Xu, W. Stable Cycling of High-Voltage Lithium Metal Batteries in Ether Electrolytes. *Nat. Energy* **2018**, *3* (9), 739−746.
(23) Wang, A. P.; Kadam, S.; Li, L. H.; Shi, S. Q.; Qi, Y. Review on Modeling of the Anode Solid Electrolyte Interphase (SEI) for Lithium-Ion Batteries. *Npj Comput. Mater.* **2018**, *4*, 15.
(24) Kamphaus, E. P.; Angarita-Gomez, S.; Qin, X. P.; Shao, M. H.; Engelhard, M.; Mueller, K. T.; Murugesan, V.; Balbuena, P. B. Role of Inorganic Surface Layer on Solid Electrolyte Interphase Evolution at Li-Metal Anodes. *ACS Appl. Mater. Interfaces* **2019**, *11*, 31467−31476.
(25) Camacho-Forero, L. E.; Smith, T. W.; Bertolini, S.; Balbuena, P. B. Reactivity at the Lithium−Metal Anode Surface of Lithium−Sulfur Batteries. *J. Phys. Chem. C* **2015**, *119*, 26828−26839.
(26) Chenoweth, K.; van Duin, A. C. T.; Goddard, W. A. ReaxFF Reactive Force Field for Molecular Dynamics Simulations of Hydrocarbon Oxidation. *J. Phys. Chem. A* **2008**, *112*, 1040−1053.
(27) Bertolini, S.; Balbuena, P. B. Buildup of the Solid Electrolyte Interphase on Lithium-Metal Anodes: Reactive Molecular Dynamics Study. *J. Phys. Chem. C* **2018**, *122*, 10783−10791.
(28) van Duin, A. C. T.; Dasgupta, S.; Lorant, F.; Goddard, W. A. ReaxFF: A Reactive Force Field for Hydrocarbons. *J. Phys. Chem. A* **2001**, *105*, 9396−9409.
(29) Bedrov, D.; Smith, G. D.; van Duin, A. C. T. Reactions of Singly-Reduced Ethylene Carbonate in Lithium Battery Electrolytes: A Molecular Dynamics Simulation Study Using the ReaxFF. *J. Phys. Chem. A* **2012**, *116*, 2978−2985.
(30) O'Hearn, K. A.; Swift, M. W.; Liu, J. L.; Magoulas, I.; Piecuch, P.; van Duin, A. C. T.; Aktulga, H. M.; Qi, Y. Optimization of the Reax Force Field for the Lithium−Oxygen System Using a High Fidelity Charge Model. *J. Chem. Phys.* **2020**, *153*, 084107.
(31) Islam, M. M.; Kolesov, G.; Verstraelen, T.; Kaxiras, E.; van Duin, A. C. T. eReaxFF: A Pseudoclassical Treatment of Explicit Electrons within Reactive Force Field Simulations. *J. Chem. Theory Comput.* **2016**, *12*, 3463−3472.
(32) Li, Y. S.; Leung, K.; Qi, Y. Computational Exploration of the Li-Electrode/Electrolyte Interface in the Presence of a Nanometer Thick Solid-Electrolyte Interphase Layer. *Acc. Chem. Res.* **2016**, *49*, 2363−2370.
(33) Liu, Y.; Yu, P. P.; Wu, Y.; Yang, H.; Xie, M.; Huai, L. Y.; Goddard, W. A.; Cheng, T. The DFT-ReaxFF Hybrid Reactive Dynamics Method with Application to the Reductive Decomposition Reaction of the TFSI and DOL Electrolyte at a Lithium−Metal Anode Surface. *J. Phys. Chem. Lett.* **2021**, *12*, 1300−1306.
(34) Liu, Y.; Sun, Q. T.; Yu, P. P.; Wu, Y.; Xu, L.; Yang, H.; Xie, M.; Cheng, T.; Goddard, W. A. Effects of High and Low Salt Concentrations in Electrolytes at Lithium−Metal Anode Surfaces Using DFT-ReaxFF Hybrid Molecular Dynamics Method. *J. Phys. Chem. Lett.* **2021**, *12*, 2922−2929.
(35) Camacho-Forero, L. E.; Balbuena, P. B. Effects of Charged Interfaces on Electrolyte Decomposition at the Lithium Metal Anode. *J. Power Sources* **2020**, *472*, 228449.
(36) Kresse, G.; Hafner, J. Ab initio Molecular-Dynamics Simulation of the Liquid-Metalamorphous-Semiconductor Transition in Germanium. *Phys. Rev. B: Condens. Matter Mater. Phys.* **1994**, *49* (20), 14251−14269.
(37) Perdew, J. P.; Burke, K.; Ernzerhof, M. Generalized Gradient Approximation Made Simple. *Phys. Rev. Lett.* **1996**, *77* (18), 3865−3868.
(38) Naserifar, S.; Oppenheim, J. J.; Yang, H.; Zhou, T. T.; Zybin, S.; Rizk, M.; Goddard, W. A. Accurate Non-Bonded Potentials Based on Periodic Quantum Mechanics Calculations for Use in Molecular Simulations of Materials and Systems. *J. Chem. Phys.* **2019**, *151*, 154111.

https://doi.org/10.1021/acsenergylett.1c00907
ACS Energy Lett. 2021, 6, 2320−2327

(39) Monkhorst, H. J.; Pack, J. D. Special Points for Brillouin-Zone Integrations. *Phys. Rev. B* **1976**, *13* (12), 5188−5192.
(40) Kresse, G.; Joubert, D. From Ultrasoft Pseudopotentials to the Projector Augmented-Wave Method. *Phys. Rev. B: Condens. Matter Mater. Phys.* **1999**, *59* (3), 1758−1775.
(41) Plimpton, S. Fast Parallel Algorithms for Short-Range Molecular Dynamics. *J. Comput. Phys.* **1995**, *117*, 1−19.
(42) Sodeyama, K.; Yamada, Y.; Aikawa, K.; Yamada, A.; Tateyama, Y. Sacrificial Anion Reduction Mechanism for Electrochemical Stability Improvement in Highly Concentrated Li-Salt Electrolyte. *J. Phys. Chem. C* **2014**, *118*, 14091−14097.
(43) Qian, J.; Baskin, A.; Liu, Z.; Prendergast, D.; Crumlin, E. J. Addressing the Sensitivity of Signals from Solid/Liquid Ambient Pressure XPS (APXPS) Measurement. *J. Chem. Phys.* **2020**, *153*, 044709.

https://doi.org/10.1021/acsenergylett.1c00907
ACS Energy Lett. 2021, 6, 2320−2327